Journal of Crystal Growth 468 (2017) 493–501

Contents lists available at ScienceDirect

Journal of Crystal Growth

journal homepage: www.elsevier.com/locate/jcrysgro

Shear flow suppresses the volume of the nucleation precursor clusters in lysozyme solutions

Michael C. Byington[a], Mohammad S. Safari[a], Jacinta C. Conrad[a,*], Peter G. Vekilov[a,b,*]

[a] Department of Chemical and Biomolecular Engineering, University of Houston, 4726 Calhoun Road, Houston, TX 77204, USA
[b] Department of Chemistry, University of Houston, 3585 Calhoun Road, Houston, TX 77204, USA

ARTICLE INFO

Communicated by Satoshi Uda

Keywords:
Solution crystallization
Protein crystals
Nucleation
Two-step nucleation mechanism
Solution flow
Nucleation suppression

ABSTRACT

Shear flow alters the rate at which crystals nucleate from solution, yet the underlying mechanisms remain poorly understood. To fill this knowledge gap, we explore the response to shear of dense liquid clusters, which may serve as crystal nucleation precursors. Solutions of the protein lysozyme were sheared in a Couette cell at rates from 0.3 to 200 s^{-1} for up to seven hours. The cluster size and total population volume were characterized by dynamic light scattering. We demonstrate that shear rates greater than 10 s^{-1} applied for longer than one hour reduce the volume of the cluster population. The likely mechanism of the observed response involves enhanced partial unfolding of the lysozyme molecules, which exposes hydrophobic surfaces between the constituent domains to the aqueous solution. We show that disruption of the intramolecular S-S bridges does not contribute to the mechanism of response to shear. The decrease of the cluster population volume with increasing shear rate or shear time implies that nucleation could be inhibited at moderate shear rates.

1. Introduction

The vast majority of solution crystallization in nature and industry occurs in flowing or stirred environments. Natural crystals, such as calcite, gypsum, quartz, and others, form in subterranean streams and reservoirs [1–3]. In typical industrial settings, crystallization is combined with synthesis, which starts and proceeds with thorough mixing of reagents [4]. Even in unstirred reactors, density gradients due to concentration and temperature non-uniformities drive buoyancy-driven convection [5]. Correspondingly, the effects of solution flow on the growth of crystals, attributed to improved solute supply to the growth interface and the formation of a hydrodynamic boundary layer along the crystal surface, have been studied since the early days of crystallization science [6–8].

By contrast, there is scarce theoretical understanding of the consequences of solution flow for crystal nucleation. Indeed, only two studies to date provide quantitative predictions of the effects of shear flow on the nucleation rate. First, calculations of enhanced transport to the nucleus due to shear flow over that of pure diffusion concluded that the faster growth rate of the nuclei, which enters the pre-exponential factor in the common nucleation rate expressions, does not significantly affect the nucleation rate [9]. Second, simulations of crystal nucleation in a melt predicted that, if the product of the shear rate and the time of monomer diffusion over a characteristic length is greater than 10^{-3}, the nucleus size and the free energy barrier for nucleation increase and nucleation is suppressed owing to shear-enforced misorientation of the incoming molecules [10]. No effect was expected for lower shear. The longest of the characteristic length scales in solution crystallization is the distance between solute molecules, of order 10 nm. With typical diffusivities of order 10^{-10} m^2s^{-1}, the respective diffusion time is about 1 μs, and the above criterion predicts that nucleation would be affected by shear rates higher than 1000 s^{-1}.

The predictions of the two theoretical studies disagree with observations on solution flow effects on crystal nucleation. Experiments with glycine revealed acceleration of nucleation by shear rates as low as 25 s^{-1}[11]. Likewise, tests aboard spacecraft, where buoyancy-driven convection is suppressed, have in many cases yielded greater or smaller numbers of nucleated crystals than earth-based laboratory controls [12–15]. The difference between earth- and space-based experiments is the presence or suppression of buoyancy driven flows. To estimate the shear rates of buoyancy-driven flow in laboratory crystallization containers, we note that prior to crystal nucleation, the density non-uniformity $\Delta\rho$ that drives convection is due to temperature gradients ΔT. The thermal expansion coefficients of aqueous solutions are typically of order 10^{-4} K^{-1}[16]. With ΔT of order 0.1 K, $\Delta\rho$ is of order 10^{-8} kg m^{-3}, inducing convection rates of order μm s^{-1} and shear rates of 0.001–0.01 s^{-1}[17–20]. This comparison suggests that shear rates of order 0.001–0.01 s^{-1} may either accelerate or suppress crystal

* Corresponding authors.
E-mail addresses: jcconrad@uh.edu (J.C. Conrad), vekilov@uh.edu (P.G. Vekilov).

http://dx.doi.org/10.1016/j.jcrysgro.2016.12.080

Available online 22 December 2016

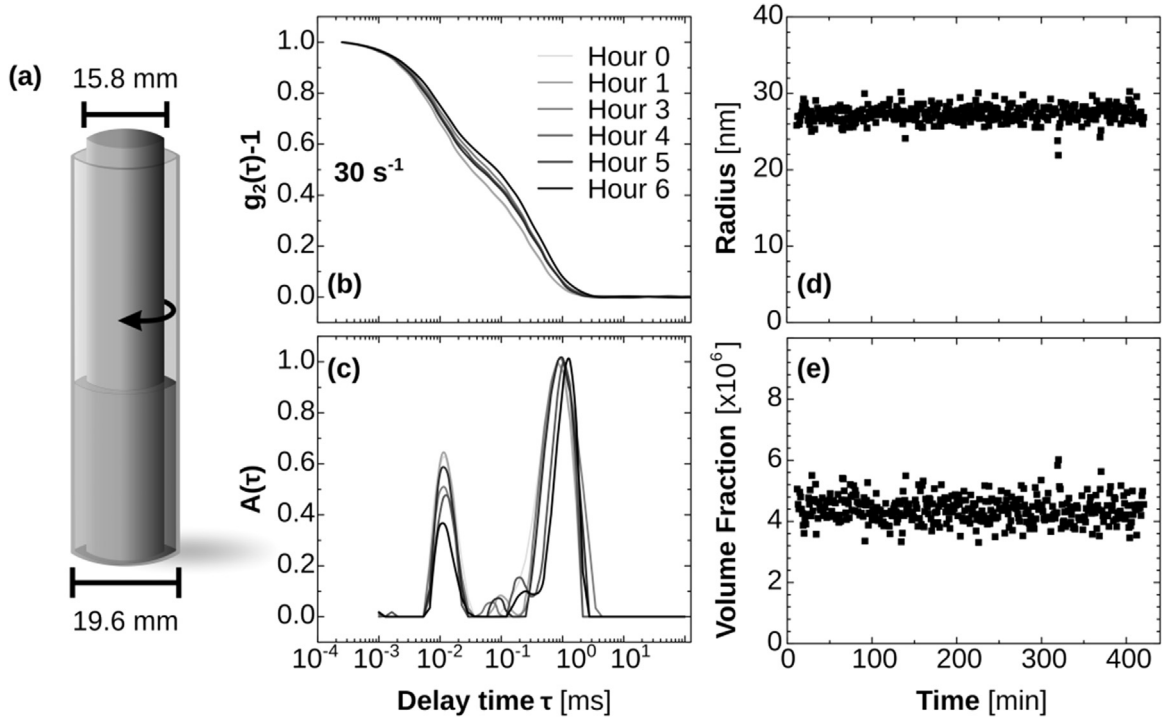

Fig. 1. (a) Schematic and dimensions of a Couette cell, consisting of a static glass barrel and concentric rotating Teflon rod. (b) Evolution of the intensity correlation functions of scattered light with time of shearing at a shear rate of 30 s^{-1} in solution. (c) Intensity distribution functions computed from the correlation functions in (b) using the CONTIN algorithm. Previous tests have demonstrated that the widths of two peaks does not reflect polydispersity of the respective scatters, but rather the non-uniform solution composition that affects the diffusivity of individual monomers and clusters [50]. The effect is amplified by intermolecular repulsion between lysozyme molecules, which leads to faster diffusion at higher concentration. (d, e) Cluster radius and volume fraction stability over time in quiescent solutions. All solutions shown here contain 100 mg mL^{-1} in 20 mM HEPES.

nucleation. Another example arises in the production of pharmaceuticals, which is often hampered by the difficulty in scaling up the crystallization conditions from laboratory containers to production multi-liter reactors. The poor scalability is often due to solution flow patterns in industrial crystallizers, which are entirely different from those in laboratory volumes [4]. An industrial reactor of meter size is stirred at a rate 0.1 m s^{-1} for a shear rate of 0.1 s^{-1}, whereas the respective values in the laboratory one-liter crystallizers are of order 1 m s^{-1} and 10 s^{-1}. A fourth example is presented by experimental tests of the effects of shear flow on crystal nucleation with the proteins ferritin, apoferritin and lysozyme [21]. The results demonstrate that the nucleation rates of ferritin and apoferritin reached a maximum at a shear rate in the range 0.01–0.1 s^{-1}, whereas that of lysozyme increased at all tested shear rates. In all four instances, the shear rates found to affect crystal nucleation are between two and four orders of magnitude lower than the theoretically predicted threshold and shear is found to not only enhance, but also suppress crystal nucleation.

In recent years, the mechanisms that lead to nucleation of crystals in solution have been the object of vigorous theoretical and experimental efforts. An important outcome was the proposal that ordered nuclei form within protein-rich clusters of concentration higher than that in the solution [22–32]. In many systems, these precursor clusters were directly observed [27,30,32–34] and the nucleation of crystal inside them, monitored [29,32,35,36]. Experiments demonstrated that greater volume of the cluster population correlates with higher nucleation rate [25,37–40]. A majority of the recent novel ideas on nucleation pathways arose from theories and experiments on protein crystallization [22,24,25,33,34,36–39]. Protein crystallization is widely employed both in the laboratory, as a critical first step in the determination of protein molecular structure by x-ray and neutron diffraction, and in industry, for preparation of biochemical reagents and pharmaceuticals [41]. Owing to the large size and slow dynamics of protein molecules, protein crystallization is a convenient model system for studies of nucleation mechanisms.

The notion that crystal nucleation follows a two-step mechanism may help to understand the experimentally observed correlations between shear and nucleation. Shear flow could potentially affect crystal nucleation within the precursor clusters in at least two ways: by enhancing or suppressing the cluster population, or by inducing shear ordering within the clusters [42,43]. Here we test the first part of the hypothesis, that shear flow affects the characteristics of the protein-rich cluster population, using experiments with the protein lysozyme. Lysozyme is one of the best-studied soluble enzymes with a robust structure, moderate size (molecular weight M_w =14,300 g mol^{-1}), and easy availability at high purity [44,45]. Nucleation rates data and direct observations suggest that lysozyme follows a two-step mechanism of crystal nucleation [24,25,36] and a population of mesoscopic protein-rich clusters that may be the nucleation precursors has been identified and characterized [46–48].

2. Materials and methods

2.1. Solution preparation

Lysozyme (Thermo Scientific #89833) used for these experiments was dissolved in deionized water containing 1.5 mM sodium azide, and, if indicated, 20 mM HEPES buffer. The solution was dialyzed against 1 L of the respective solvent using dialysis cassettes with 2000*g* mol^{-1} cutoff for 38–48 h in a refrigerator (4 °C) on a stir plate at ~50 rpm with a 2" magnetic stir bar. The beaker (1–2 L) used for dialysis was covered with parafilm to prevent evaporation. The solution was removed from the dialysis cassettes and filtered through syringe filters with 30 mm diameter and 220 nm pore size. The concentration was determined by diluting an aliquot of the prepared solution 1000-fold and measuring the absorption at 280 nm.

2.2. Solution shearing

Shear experiments were performed immediately after solution preparation using a shear cell constructed as in Fig. 1a with 20 mL glass syringe and 5/8" Teflon rod. To ensure the rod remained centered at the bottom of the syringe, the end of the rod was machined to fit the inner tip profile of the syringe. Teflon rod was rotated by a DC motor (Amico Model RC385SAP-2173-57) and DC power source (Dr. Meter HY1803D). The shear rate was set by the voltage applied to the DC motor. Shear rate and voltage were calibrated by counting the rotations in a 60 sec interval at various voltages (1.5–11 V, 0.5 V increments) then computing the shear rate in the bulk fluid assuming a linear velocity profile and no slip boundary conditions.

Shearing started immediately after solution preparation. In experiments using mercaptoethanol or urea, the respective reagent was added immediately before the start of shearing. Every hour, a 300 μL solution aliquot was removed from the shear cell. This solution sample was filtered through a 13 mm 220 nm cutoff syringe filter directly into a DLS cuvette, capped with parafilm, and loaded into the sample holder of the light scattering device.

2.3. Characterization of the cluster population

Light scattering data were collected on an instrument by ALV-GmbH, Langen, Germany, equipped with He-Ne laser operating at 632.8 nm, and an ALV-5000 EPP Multiple tau Digital Correlator. At least 10 correlation functions of 60 seconds were collected. The intensity-intensity correlation functions $g_2(\tau)$, where τ is the lag time, recorded after shearing for up to six hours, all possess two distinct shoulders, indicating the presence of two populations of scatters (Fig. 1b). The corresponding intensity distribution functions, computed using the CONTIN algorithm (Fig. 1c), indicate that both scattering populations are relatively monodisperse. To extract the cluster radius and volume fraction from DLS data [49], we fit the correlation functions with

$$g_2(\tau)-1=\left[A_1\exp\left(-\frac{\tau}{\tau_1}\right)+A_2\exp\left(-\frac{\tau}{\tau_2}\right)\right]^2+\varepsilon,$$

where the times τ_1 and τ_2 characterize the diffusion of monomers and clusters, respectively; A_1 and A_2 are amplitudes, which are proportional to the intensity scattered by the monomers and clusters, respectively, and ε accounts for mechanical, optical and electronic noise in the signal [33,50].

The parameters τ_1, τ_2, A_1, A_2, and ε were evaluated by non-linear curve fitting using SciPy (scipy.optimizize.minimize) routine. The minimized function was the squared deviation of the model from the data, multiplied by a weight function, which enhances the lower magnitude values, occurring at longer delay times.

$$f_{\mathrm{SSE}}=\sum_{\tau=\tau_{\min}}^{\tau_{\max}}\left[g_{2_{\mathrm{model}}}-g_{2_{\mathrm{data}}}\right]^2 w(\tau),$$

$$w(\tau)=\begin{cases}11.45\times\log(\tau)+87.6 & \tau<0.52\ \mathrm{ms}\\ 1 & \tau\geq 0.52\ \mathrm{ms}\end{cases}.$$

Here $\tau_{\max}$ is the value beyond which the correlation function decays below 10^{-5} and $\tau_{\min}$ is 1.25×10^{-4} ms, the shortest time accessible by the ALV detector. As defined, $w(\tau)\geq 1$ for all τs. The weight function was chosen for simplicity: for $\tau<0.52$ ms it corresponds to multiplying each element of the array of squared deviations by its index (note that delay times recorded by the ALV detector are not equally spaced in time). The use of a weight function ensures that the values of a correlation function at long times, which may be one or two orders of magnitude lower than those at shorter times, contribute to the fit.

The parameter ε, which account for the noise, was one or two orders of magnitude lower than amplitudes A_1 and A_2. From τ_1, τ_2, A_1, and A_2 we compute the cluster size R_2, the hydrodynamic radius of the monomer R_1, used for verification of the experimental procedures, and the fraction of the solution volume occupied by the cluster population ϕ_2. For R_i (i=1, 2) we use the Stokes-Einstein relation,

$$R_i=\frac{k_BTq^2}{6\pi\eta_i}\tau_i,$$

where η_2=1.42mPa•s is the viscosity of the solution through which clusters diffuse and η_1=1.025mPa•s is the viscosity of the solvent through which the monomers diffuse. The temperature was set at T=297. 65K and k_B is the Boltzmann constant.

We evaluate ϕ_2 from [33,50]

$$\phi_2=\frac{A_2}{A_1}\frac{1}{P(qR_2)f(C_1)}\frac{(\partial n/\partial C_1)_{T,\mu}}{(\partial n/\partial C_2)_{T,\mu}}\left(\frac{\rho_1}{\rho_2}\right)^2\left(\frac{R_1}{R_2}\right)^3\phi_1.$$

Here $q=\frac{4\pi n_0\sin(\theta/2)}{\lambda}=1.87\times10^7\,\mathrm{m}^{-1}$ is the scattering wave vector of light with wavelength $\lambda=632.8$ nm at scattering angle $\theta=90°$; n_0 =1.331 as the solvent refractive index. $P(qR_2)=\frac{3}{(R_2q)^3}[\sin(R_2q)-R_2q\cos(R_2q)]^2$ is the shape factor assuming a spherically shaped cluster. The function $f(C_1)$ accounts for the intermolecular interactions between monomers, which depends on the monomer concentration C_1; it was determined by static light scattering and at C_1 =100 mg mL^{-1}, tested here, $f(C_1)$=4[46]. The ratios $\partial n/\partial C_1$ and $\partial n/\partial C_2$ are the increments of the solution refractive index n with the concentrations of monomers, C_1, and clusters, C_2. Since in these ratios both concentrations are in units mass per unit volume, we assume $\frac{(\partial n/\partial C_1)_{T,\mu}}{(\partial n/\partial C_2)_{T,\mu}}\approx 1$. ρ_1 and ρ_2 are the mass densities of the protein monomer and the clusters, respectively. We assume that ρ_1=1.3 g cm^{-3}[51], and ρ_2=0.45 g cm^{-3}, the protein concentration in the clusters, which is likely close to the concentration in the stable dense protein liquid at similar conditions [48,52]. ϕ_1 is the fraction of the solution volume occupied by monomers, calculated from their mass concentration C_1 as $\phi_1=C_1\upsilon_pN_A/M_w$, where $\upsilon_p=2.0\times10^{-20}$ cm^3 is the molecular volume in solution [51]. Thus, for C_1 =100 mg mL^{-1} we get ϕ_1 =0.084.

In plots where R_2 or ϕ_2 are averaged over several data points, they are plotted as a function of the time of the first datum point.

2.4. Determination of enzyme activity

Activity was measured by monitoring the rate of absorbance decrease at 450 nm[2] in a solution of 0.01 mg mL^{-1} lysozyme and *Micrococcus lysodeikticus* (M3770 Sigma) at an optical density of 0.33. A 200 μL solution was prepared for each sample and monitored in a 96 well plate reader for 5 min. The changes in the rate of absorbance decrease indicate changes in the number of functional active sites in solution.

2.5. Characterization of protein structural integrity

The conformational integrity of lysozyme was tested using the 1-anilino-8-naphthalenesulfonate (ANS) and Thioflavin T (ThT) assays. ANS was dissolved at 13 mM in 20 mM HEPES at pH=7.8. The solution was filtered through a 0.2 μm Teflon filter. The ANS concentration was determined spectrophotometrically using extinction coefficient 18 mM^{-1} cm^{-1} at 270 nm [53]. 20 μL of this solution were added to 20 μL of the tested lysozyme solution and diluted with 160 μL of 20 mM HEPES to a total volume of 200 μL [53]. For experimental statistics, five identical samples of this solution mixture were loaded in a multi-well plate and the florescence response to excitation at 350 nm was recorded between 400 and 650 nm (with an increment of 5 nm) by an Infinite 200 PRO microplate reader (Tecan). ThT was dissolved at 6 mM in 20 mM HEPES at pH=7.8. As with ANS, the solution was filtered through a 0.2 μm Teflon filter. The ThT concentration was

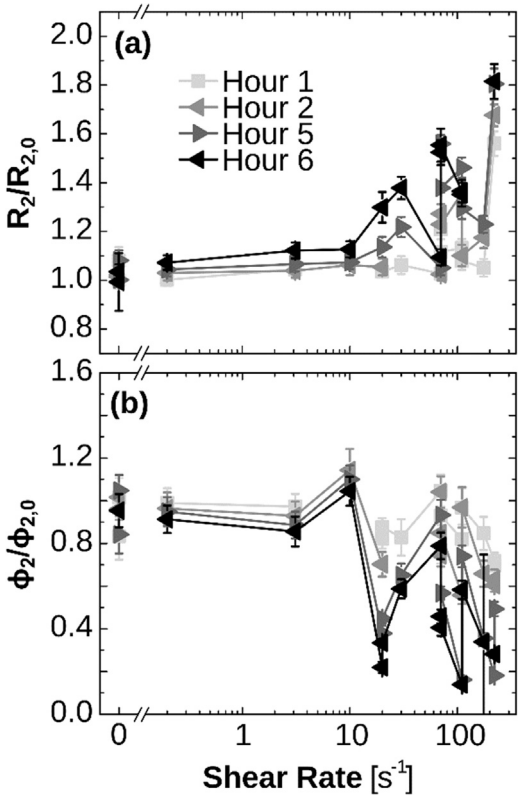

Fig. 2. (a) Variation of the cluster radius R_2, scaled with that in unsheared solutions $R_{2,0}$, with increasing shear rate after shearing for times indicated in 20 mM HEPES buffer and 100 mg mL^{-1} lysozyme. (b) Variation in the fraction of solution occupied by the cluster volume ϕ_2 at the same conditions scaled by the quiescent cluster volume fraction $\phi_{2,0}$.

determined spectrophotometrically using extinction coefficient 26.6 mM^{-1}cm^{-1} at 416 nm [53]. 1 μL of this solution was added to 20 μL of the tested lysozyme solution and diluted with HEPES to 200 μL [53]. Five identical samples of this solution mixture were loaded in a multi-well plate and the florescence response to excitation at 442 nm was recorded between 472 and 650 nm (with an increment of 2 nm) by an Infinite 200 PRO microplate reader (Tecan).

3. Results and discussion

3.1. Shear flow effects on the cluster population

In quiescent solutions both R_2 and ϕ_2 are constant over seven hours (Fig. 1d and e). The evolution of R_2 and of ϕ_2 in solutions buffered with HEPES at shear rates varying from 0.3 to 200 s^{-1} are displayed in Fig. 2a and b. The enforced shear rates are much larger than that induced by buoyancy-driven convection, estimated above to be in the in the range 0.001–0.01 s^{-1}. In Fig. 2a and b we scale R_2 and ϕ_2 by the corresponding values in quiescent solutions, $R_{2,0}$ and $\phi_{2,0}$. The data in these figures reveal that the lowest enforced shear rate, 0.3 s^{-1}, consistently induces a small increase in the cluster radius R_2 and a small decrease in cluster population volume ϕ_2. This effect increases at longer exposures to shear, but is always limited to less than 10% of $R_{2,0}$ and $\phi_{2,0}$. Exposures to shear rates lower than a threshold value do not induce additional deviations of R_2 and ϕ_2 from their values in quiescent solutions. After this threshold is reached, however, R_2 increases and ϕ_2 decreases as a function of increasing shear rate. While the threshold shear rate is mostly unaffected by the duration of shearing, longer exposure to shear above the threshold amplifies the effects of faster shearing. At shear rates faster than 100 s^{-1}, the solution remained turbid even after filtering through a 0.22 μm filter, suggesting irreversible denaturation and aggregation of a part of the dissolved protein.

3.2. Partial protein unfolding as part of the mechanism of response to shear

The negatively coupled response of R_2 and ϕ_2 to increasing shear is in contrast to conventional phase transformations—such as solidification or liquefaction—in which the domain size of the incipient phase increases concurrently with its overall volume in response to variations of the external parameters. To understand the mechanism that underlies the surprising trends observed with the protein-rich clusters, we compare the effects of shear in solutions of three compositions: HEPES buffer, used in the experiments displayed in Fig. 2a and b, water, in Fig. 3a and b, and urea, in Fig. 3c and d. HEPES (sodium 2-[4-(2-hydroxyethyl)piperazin-1-yl]ethanesulfonate) is a zwitterionic organic molecule that is used to maintain near-physiological pH. Binding of the HEPES solution species to proteins is extremely rare [54], suggesting that its action on the cluster properties would be through the hydrogen ion concentration, adjusted to pH=7.8. If lysozyme is dissolved in water and dialyzed to remove the excess precipitant used in purification, pH sets at 5.4. Protonation of basic and acidic surface aminoacid groups leads to a +8 net charge of the lysozyme monomer at pH=7.8 [55,56], the balance of 17 positive and nine negative groups [56]. At the lower pH=5.4, the net charge increases to +12 [55]. The data in Figs. 2a and b and 3a and b reveal that the change from HEPES buffer to water induces stronger sensitivity to shear: the threshold shear rate for increased R_2 and lowered ϕ_2 decreases from 10 s^{-1} to 3 s^{-1}. A possible explanation for the effects of solution composition on the response to shear is that the higher molecular charge increases repulsion between intramolecular domains and hence destabilizes the molecular conformation.

To test the correlation between molecular destabilization and response to shear, we studied the effects of shear on the cluster population in urea-containing solutions. Urea is known to perturb the native structure of most proteins; addition of 8 M urea to aqueous solutions completely unfolds proteins [57–59]. Urea is currently thought to be a universal denaturant because it interacts favorably with the peptide backbone [60]. The aminoacid side chains further assist the action of urea by additional preferential interaction with it and by diluting the effective concentration of the backbone amides [61–63]. The accumulation of urea at non-polar protein patches and the accompanying destruction of the water structures are described as chaotropic action [64]. The addition of 1 M urea to a lysozyme solution in 20 mM HEPES buffer preserves the pH at 7.8. Nonetheless, the data in Fig. 3c and d reveal that adding urea reduces the threshold for enhanced response to shear from 10 to 3 s^{-1}, supporting partial protein unfolding as a contributor to the cluster population response to solution shear.

The suggested conformational destabilization implies an explanation of the non-monotonic responses of R_2 and ϕ_2 to higher shear observed in Figs. 2 and 3. In other experiments under identical conditions, we found that, overall, R_2 always increased and ϕ_2 always decreased at faster shear rates and longer exposures to shear. The threshold shear rates for these trends were faithfully reproduced. Non-monotonic behaviors, however, were observed at varying shear rates above the threshold, or not at all. We conclude that after the native protein conformation is destabilized by shearing faster than the threshold rate, the degree of induced partial unfolding may vary in response to minor inconsistencies in the system parameters.

Previous investigations of the protein-rich clusters in lysozyme solutions revealed several behaviors that sharply contrast with established laws of phase transitions: sizes much larger than the prediction of a colloid clustering scenario (which assumes structurally intact molecules) [65], decoupled responses of cluster population volume and cluster size to variations in ionic strength, pH, and additive

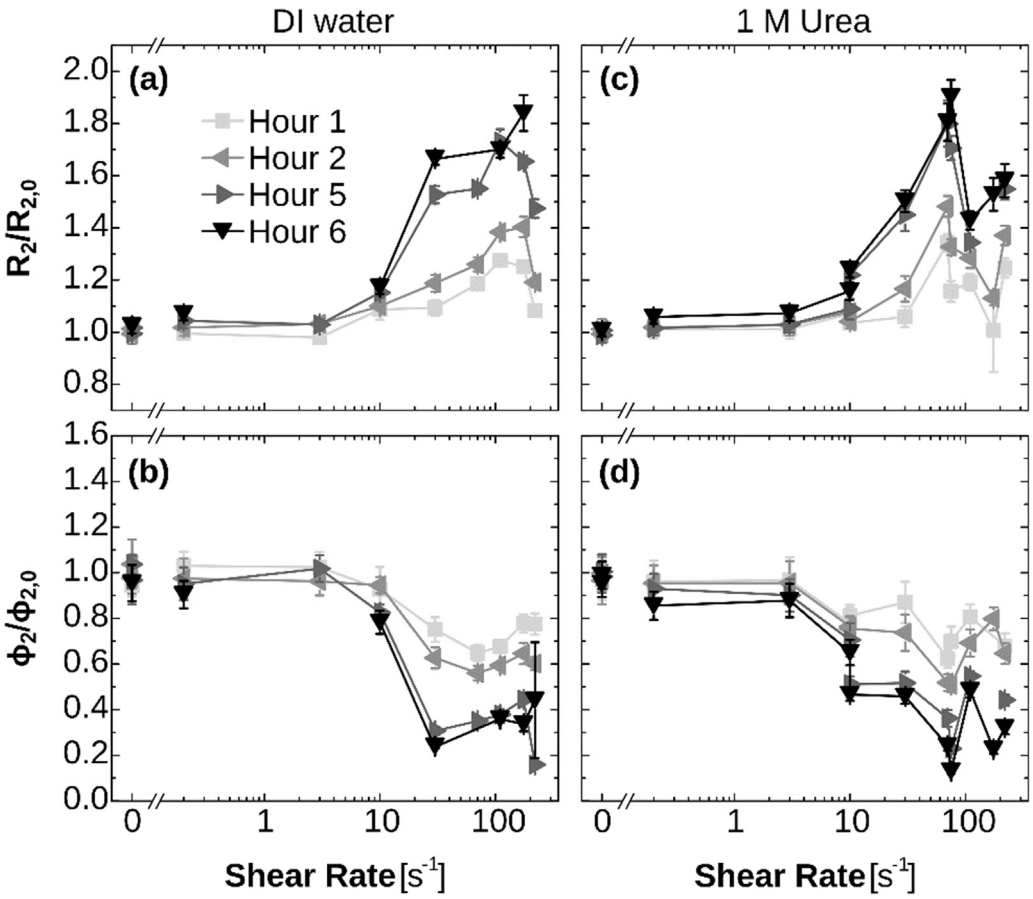

Fig. 3. (a) Variation of the cluster radius R_2, scaled with that in unsheared solutions $R_{2,0}$, with increasing shear rate after shearing for times indicated in DI water and 100 mg mL^{-1} lysozyme. (b) Variation in the fraction of solution occupied by the cluster volume ϕ_2 at the same conditions scaled by the quiescent cluster volume fraction $\phi_{2,0}$. (c,d) Same variation in radius and volume fraction of lysozyme clusters in 100 mg mL^{-1} lysozyme, 1 M Urea, and 20 mM HEPES for times indicated in (a).

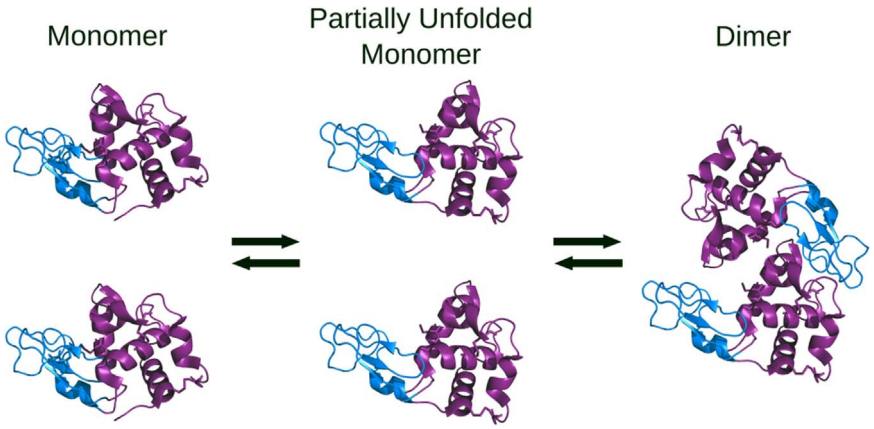

Fig. 4. Schematic representation of the proposed partial unfolding mechanism for dimerization of lysozyme in solution. The structural domains of lysozyme (α and β) are highlighted in purple and blue, respectively. The domains are linked by two peptide chain loops and a S–S bridge (indicated with arrows) that are aligned in a hinge, which allows domains to open and hence expose the nonpolar interdomain interface to the solution. Hydrophobic attraction between internal domain surfaces from different molecules leads to domain-swapped oligomers. Protein structure drawn using PyMOL and atomic coordinates from Wang et al. [69]; α and β domains identified as in McCammon et al. [70].

concentration, and decreased cluster population volume upon stronger intermolecular attraction [46, 66, 67]. These responses indicate that the mesoscopic clusters represent a novel class of protein condensate that forms by a fundamentally different mechanism than other protein aggregates, such as crystals and amyloid fibrils. The available data suggest that the clusters form by the accumulation of transient protein oligomers [48, 68]. Experiments with lysozyme indicate that the lysozyme oligomers are domain-swapped dimers or trimers, linked by hydrophobic bonds between the peptide backbones exposed to the solvent after partial unfolding of the lysozyme molecule, illustrated in Fig. 4 [46, 66].

The oligomer mechanism of cluster formation in lysozyme solutions explains how shear affects the cluster population through partial protein unfolding. According to theory, the cluster size is related to the diffusivity D_{oligo} and decay rate constant k_{oligo} of domain-swapped oligomers as $R_2 = \sqrt{D_{oligo}/k_{oligo}}$ [48, 68]. There are two mechanisms by which shear flow could increase the cluster size. First, solution flow may accelerate the exodus of oligomers from the clusters, effectively increasing D_{oligo}. With oligomer diffusivity of order 10^{-10} m^2 s^{-1}

(comparable to that of the monomer), diffusion over the cluster radius of about 30 nm would have a characteristic time of about 10 μs. This is nearly three orders of magnitude faster than oligomer transport enhanced by shear rates slower than 200 s^{-1}, which have characteristic times longer than 5 ms. This estimate suggests that the second mechanism, involving shear-induced unfolding, dominates. The unfolding slows the decay rate of oligomers k_{oligo} and hence increases the cluster size. This mechanism is supported by the stronger response to shear in the presence of urea and at lower pH, both of which destabilize the native protein conformation, in Fig. 3. Furthermore, because the cluster population volume is determined by the free-energy balance between clusters and solution [47], the decrease in ϕ_2 is likely due to stronger attraction between lysozyme molecules with exposed nonpolar interdomain surfaces in a partially unfolded conformation, which lowers the chemical potential of the protein in the solution. Importantly, the cluster population response to mechanical unfolding, by shearing, opposes that to chemical unfolding, by urea [46]. Urea weakens the hydrophobic interaction between newly exposed nonpolar patches. This chaotropic effect decreases the oligomer lifetime and increases the solution free energy, inducing *smaller* clusters and *larger* cluster populations.

3.3. Are broken disulfide bridges necessary for cluster formation?

An important question both for the general mechanism of protein-rich clusters and the specific mechanism of shear effects on the cluster population is whether intramolecular S-S bridges are disrupted during the unfolding leading to clusters. The lysozyme structure in Fig. 4 suggests that the formation of domain-swapped lysozyme oligomers does not require the breaking of S-S bridges. To answer this question we partially reduced the S-S bridges with mercaptoethanol (HSC_2H_4OH, ME) and monitored the response of the cluster population in quiescent and sheared solutions. Tests revealed that four-fold molar excess of ME denatures lysozyme, whereas using 0.5 M equivalents insignificantly affects the characteristics of the cluster population. Hence, we used a molar concentration of ME equal to that of lysozyme, 6.9 mM. Previous experiments with ethanol, a reagent whose structure, polarity, and chaotropic activity are similar to those of ME, demonstrated that ethanol weakly affects the cluster population characteristics at concentrations as high as 2.5 M [46]. Hence, we expect that ME only affects the clusters through the reduction potential of the HS-group.

In quiescent solutions in the absence of ME, the cluster radius and population volume are steady (Fig. 5, in agreement with Fig. 1d and e). Shearing in pure lysozyme increases R_2 and reduces ϕ_2, in agreement with the trends observed in Figs. 2 and 3. The decrease in R_2 after 350 min of shearing at 70 s^{-1} is likely due to incipient irreversible denaturation. In quiescent solutions, ME does not affect the cluster size and induces a slow increase of the cluster population volume. These observed responses dramatically differ from those caused by significantly higher concentrations of two chaotropic agents, urea (Fig. 3c and d) or ethanol [46], suggesting that ME induces chemical and conformational changes in the lysozyme molecule that are distinct from exposure of the interdomain interface. These responses are compatible with disruption of the S-S bridges in the α or β domains (see Fig. 4), which creates disordered chain segments. The modified molecular surface leads to enhanced attraction at short intermolecular separations that lowers the free energy of the cluster phase and hence increases the cluster population volume. These newly created attractive patches may be distant from the interdomain interface; in this case they would not affect the stability and decay rate of domain-swapped oligomers, leaving the cluster size intact.

The response of the cluster population to shear in the presence of ME is similar to that in pure lysozyme solution: the cluster size increases and the cluster population volume is reduced. In the presence of ME, R_2 increases to reach a local maximum at an intermediate shearing time and decreases at longer shearing times. This trend is similar to the decrease of R_2 after shearing for 350 min at 70 s^{-1}, suggesting that it is due to ME-induced irreversible denaturation of the protein. Overall, the effects of solution shearing and ME are dissimilar, indicating that the mechanisms of cluster response to solution shear and to addition of ME are distinct. Importantly, this observation indicates that disruption of S-S bridges and the structure of the two lysozyme domains are not parts of the general mechanism of cluster formation in lysozyme or that of the response of the cluster population to shear.

3.4. The effects of shear on the cluster-solution equilibrium

Previous studies of lysozyme clusters in quiescent solutions have indicated that the clusters are in equilibrium with the monomeric protein and respond to variations of the monomer concentration as predicted by the Boltzmann relation [47,48]. In this context, a relevant question is whether the shear-modified cluster population remains in equilibrium with the lysozyme monomers. To address this issue, we sheared a lysozyme solution for 280 min at 30 s^{-1} and monitored the evolution of R_2 and ϕ_2 at quiescent conditions for 15 h after cessation of shearing. The results in Fig. 6a and b indicate that the increased R_2 and lowered ϕ_2 persist. The observed irreversibility of the cluster population characteristics may indicate either that the clusters have converted to irreversible protein aggregates, or that shear has modified the equilibrium between monomers and clusters. To distinguish between these two scenarios, we tested the response of the clusters to decreasing protein concentration from 100 to 50 and 25 mg mL^{-1} after shearing for two or four hours at 30^{-1}. The results in Fig. 6c and d indicate that R_2 does not depend on the protein concentration (in agreement with previous observations) [47,48] and this behavior is not altered by shearing. If the clusters were irreversible aggregates, the ϕ_2/ϕ_1 ratio would not depend on the solution dilution. Fig. 6d demonstrates that the ϕ_2/ϕ_1 ratio strongly decreases upon solution dilution, in sharp contrast with this expectation. This observation indicates that the clusters retain their reversibility after shearing. The surprising conclusion is that the shear-induced suppression of the cluster population volume is at least partially due to a permanent conformational modification of the monomers, with which the clusters are in equilibrium.

3.5. Tests of conformational modification as a prerequisite for cluster formation

To evaluate the magnitude of the shear-induced conformational modification, we compared the activity of lysozyme in degradation of *Micrococcus lysodeikticus* bacteria in quiescent solution and after shearing. Lysozyme hydrolyzes a tetrasaccharide found in Gram-positive bacteria and breaks the glycosidic bond between n-acetylmuramic acid and n-acetylglucosamine [71]. We observed (Fig. 7a) that the activity of lysozyme is not affected by shearing. As the active center of lysozyme consists of aminoacid residues that belong to both domains, these observations suggest that the configuration of the α and β domains of lysozyme is not affected in the majority of the solute molecules.

The conformational integrity of lysozyme after shearing was tested using the 1-anilino-8-naphthalenesulfonate (ANS) and Thioflavin T (ThT) assays. ANS is a fluorescent probe for the detection of partially unfolded states. ANS binds to buried hydrophobic sites of proteins, resulting in a blue shift of the fluorescence emission maximum and increase of the fluorescence intensity [72,73]. ThT is employed for selectively staining and identifying amyloid structures as ThT binding to β structures enhances its fluorescence emission [74]. Fig. 7b and c demonstrates that shearing does not affect the fluorescence spectra in solutions of lysozyme and each of the two probe molecules, indicating that shear-induced conformational modifications are minor.

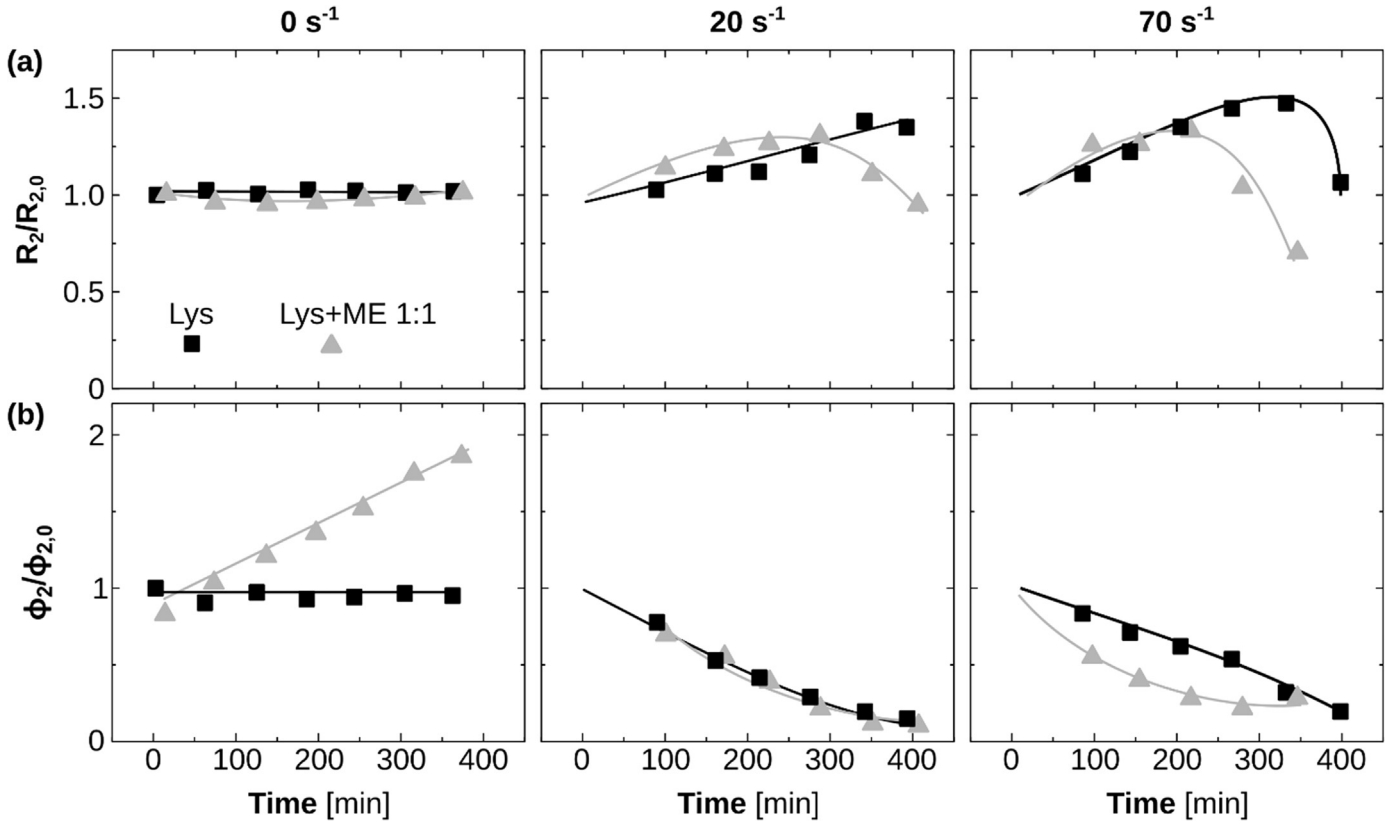

Fig. 5. Effects of mercaptoethanol (ME) on the response of lysozyme clusters to shear. Evolution of (a) average cluster radius R_2 and (b) cluster population volume ϕ_2, scaled by their respective values in quiescent solutions in the absence of ME, $R_{2,0}$ and $\phi_{2,0}$, in quiescent solution (0 s^{-1}) and at two shear rates (20 s^{-1} and 70 s^{-1}).

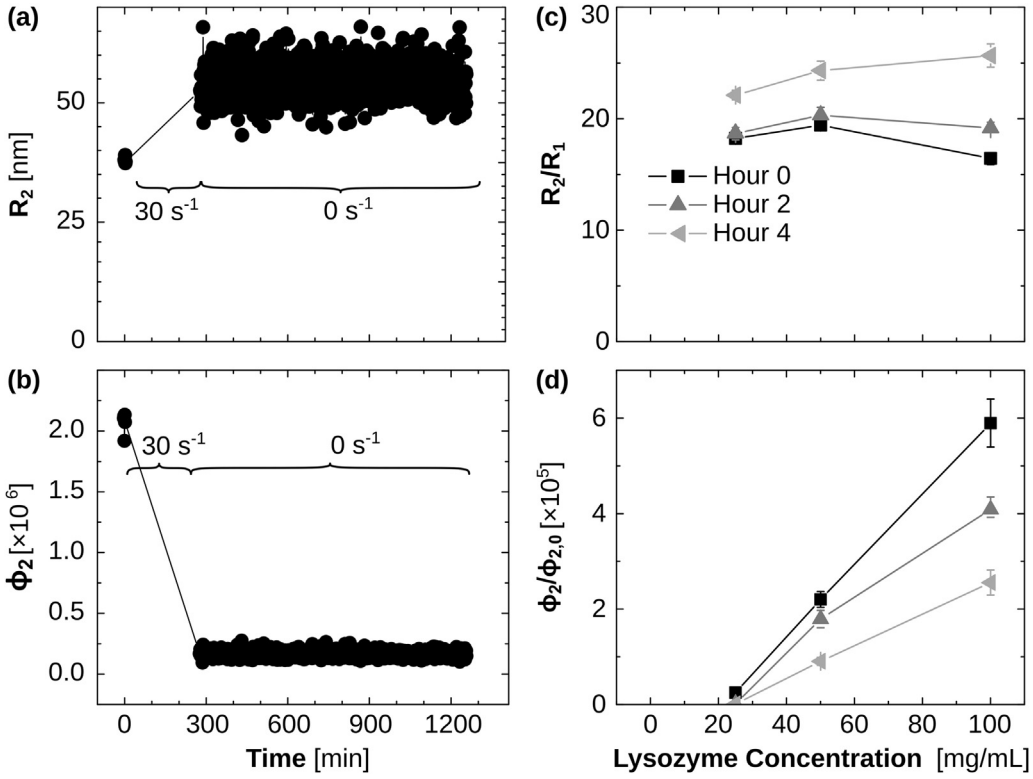

Fig. 6. Reversibility of shear effects on cluster formation. (a) Evolution of the cluster radius R_2 and (b) population volume ϕ_2 in a quiescent lysozyme solution in 20 mM HEPES buffer after 280 min of shearing at 30 s^{-1}. Values of R_2 and ϕ_2 prior to shearing are shown for comparison. (c) Variation of R_2 and (d) ϕ_2, scaled by the respective values for the monomer R_1 and ϕ_1, in an unsheared solution and solutions sheared at 30 s^{-1} for 3 and 6 h, respectively, upon sequential dilution from 100 mg mL^{-1} to 50 mg mL^{-1} and 25 mg mL^{-1}.

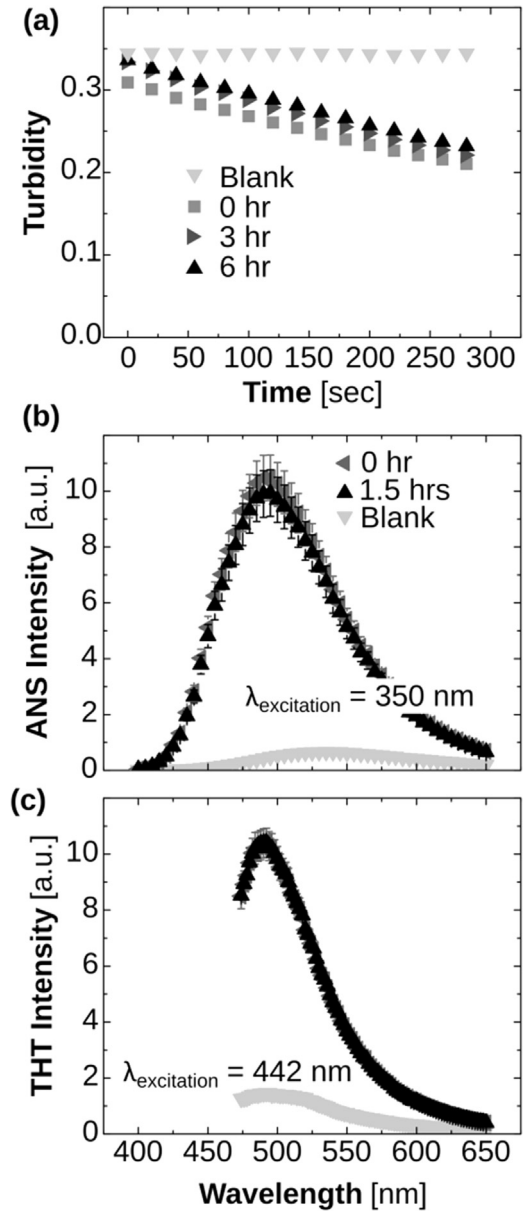

Fig. 7. (a) Evaluation of lysozyme activity in a quiescent solution and after shearing for 3 and 6 h. The absorbance at 450 nm of a suspension of the bacterium *Micrococcus lysodeikticus* decreases as lysozyme degrades the bacteria. The slopes of the dependences characterize the enzyme activity. (b) Tests of lysozyme conformation integrity using 1-anilino-8-naphthalenesulfonate (ANS) and (c) Thioflavin T (ThT). Fluorescence spectra of lysozyme solutions in the presence of the respective probe molecule upon excitation with 350 nm in (b) or 442 nm (c) in quiescent solutions and after shearing at 70 s^{-1} for 90 min are compared to the solutions containing only the respective probe molecules.

The preservation of the enzymatic activity after shearing and the unmodified fluorescence spectra in the presence of ANS and ThT suggest that the partial unfolding, which exposes sufficient hydrophobic areas of the interdomain interface to drive reduction of the cluster population volume, affects only a small fraction of the protein molecules.

4. Conclusions

We demonstrate that in solutions of the protein lysozyme shear flow increases the size and suppresses the volume of the population of protein-rich clusters that may be precursors to crystal nucleation. The likely mechanism of the observed shear response involves partial unfolding of the lysozyme molecules, which exposes to the aqueous solution the non-polar interfaces between the constituent α and β domains. The extended hydrophobic surfaces lower the chemical potential of the lysozyme in the solution and, per the oligomer mechanism of cluster formation [46–48, 66], stabilize a domain-swapped oligomer. The former outcome lowers the volume occupied by the cluster phase, whereas the latter increases the cluster radius. Experiments in which the intramolecular S-S bridges are reduced by mercaptoethanol indicate that disruption of the domain structure is not a part of the mechanism of response to shear.

In the broader context of shear flow effects on crystal nucleation, the observation of decreased cluster population volume at shear rates of order 10 s^{-1} implies that nucleation should be inhibited at these shear rates. This is the first prediction of nucleation suppression in response to shear, elicited by unexpectedly moderate shear rates. On the other hand, the experimentally-observed enhancement of nucleation at shear rates of order 0.1 s^{-1} does not correlate with changes in cluster properties and suggests that alternative mechanisms, such as shear ordering inside the clusters, may be active.

Acknowledgments

We thank Maria A Vorontsova and J. Lutsko for helpful suggestions on the experiments and result interpretation. Funding was generously provided by NASA (Grants NNX14AE79G and NNX14AD68G).

References

[1] F. Lippmann, Sedimentary Carbonate Minerals, Springer-Verlag Berlin Heidelberg, 1973.
[2] J.M. García-Ruiz, R. Villasuso, C. Ayora, A. Canals, F. Otálora, Formation of natural gypsum megacrystals in Naica, Mexico, Geology 35 (2007) 327–330.
[3] J.W. Anthony, Handbook of Mineralogy, Mineral Data Publishing, 1997.
[4] A.S. Myerson, Handbook of Industrial Crystallization, 2nd ed., Butterworth-Heinemann, Woburn, MA, 2001 (Paperback).
[5] E. Chassignet, C. Cenedese, J. Verron, Buoyancy-Driven Flows, Cambridge University Press, Cambridge, 2012.
[6] H.E. Buckley, Crystal Growth, John Wiley & Sons, Inc., New York, 1951.
[7] A.A. Chernov, The spiral growth of crystals, Sov. Phys. Uspekhi 4 (1961) 116–148.
[8] A.A. Chernov, Modern Crystallography III, Crystal Growth, Springer, Berlin, 1984.
[9] D. Reguera, J.M. Rubí, Homogeneous nucleation in inhomogeneous media. II. Nucleation in a shear flow, J. Chem. Phys. 119 (2003) 9888.
[10] R. Blaak, S. Auer, D. Frenkel, H. Löwen, Homogeneous nucleation of colloidal melts under the influence of shearing fields, J. Phys.: Condens. Matter 16 (2004) S3873–S3884.
[11] C. Forsyth, P.A. Mulheran, C. Forsyth, M.D. Haw, I.S. Burns, J. Sefcik, Influence of controlled fluid shear on nucleation rates in glycine aqueous solutions, Cryst. Growth Des. 15 (2015) 94–102.
[12] K. Asano, S. Fujita, T. Senda, Y. Mitsui, Crystal growth of ribonuclease S under microgravity, J. Cryst. Growth 122 (1992) 323–329.
[13] G.E.O. Borgstahl, A. Vaherdi-Faridi, J. Lovelace, H.D. Bellamy, E.H. Snell, Atest for macromolecular crystallization in microgravity: large well ordered insulin crystals, Acta Cristallogr. Sect. D 57 (2001) 1204–1207.
[14] C.E. Kundrot, R.A. Judge, M.L. Pusey, E.H. snell, Microgravity and macromoleular crystallography, Cryst. Growth Des. 1 (2001) 87–99.
[15] R. Hilgenfeld, A. Liesum, R. Strom, A. Plaas-Link, Crystallization of two bacterial enzymes on an unmanned space mission, J. Cryst. Growth 122 (1992) 330–339.
[16] L.G. Hepler, Thermal expansion and structure in water and aqueous solutions, Can. J. Chem. 47 (1969) 4613–4617.
[17] H. Lin, D.N. Petsev, S.-T. Yau, B.R. Thomas, P.G. Vekilov, Lower incorporation of impurities in ferritin crystals by suppression of convection: modeling results, Cryst. Growth Des. 1 (2001) 73–79.
[18] H. Lin, F. Rosenberger, J.I.D. Alexander, A. Nadarajah, Convective-diffusive transport in protein crystal growth, J. Cryst. Growth 151 (1995) 153–162.
[19] M. Pusey, W. Witherow, R. Naumann, Preliminary investigation into solutal flow about growing tetragonal lysozyme crystals, J. Cryst. Growth 90 (1988) 105–111.
[20] K. Onuma, K. Tsukamoto, S. Nakadate, Application of real time phase shift interferometer to the meaurement of concentration field, J. Cryst. Growth 123 (1993) 706–718.
[21] A. Penkova, W. Pan, F.V. Hodjaoglu, P.G. Vekilov, Enhancement and suppression of protein crystal nucleation under the influence of shear flow, Ann. N. Y. Acad. Sci. 1077 (2006) 214–231.
[22] P.R. ten Wolde, D. Frenkel, Enhancement of protein crystal nucleation by critical density fluctuations, Science 277 (1997) 1975–1978.
[23] V. Talanquer, D.W. Oxtoby, Crystal nucleation in the presence of a metastable critical point, J. Chem. Phys. 109 (1998) 223–227.
[24] O. Galkin, P.G. Vekilov, Control of protein crystal nucleation around the metastable liquid-liquid phase boundary, Proc. Natl. Acad. Sci. USA 97 (2000) 6277–6281.

[25] P.G. Vekilov, Nucleation, Cryst. Growth Des. 10 (2010) 5007–5019.
[26] P.G. Vekilov, Dense liquid precursor for the nucleation of ordered solid phases from solution, Cryst. Growth Des. 4 (2004) 671–685.
[27] D. Gebauer, M. Kellermeier, J.D. Gale, L. Bergstrom, H. Colfen, Pre-nucleation clusters as solute precursors in crystallisation, Chem. Soc. Rev. (2014).
[28] D. Gebauer, A. Volkel, H. Colfen, Stable Prenucleation Calcium Carbonate Clusters, Science 322 (2008) 1819–1822.
[29] E.M. Pouget, P.H.H. Bomans, J.A.C.M. Goos, P.M. Frederik, G. de With, N.A.J.M. Sommerdijk, The initial stages of template-controlled CaCO3 formation revealed by cryo-TEM, Science 323 (2009) 1455–1458.
[30] A. Dey, P.H.H. Bomans, F.A. Müller, J. Will, P.M. Frederik, G. de With, N.A.J.M. Sommerdijk, The role of prenucleation clusters in surface-induced calcium phosphate crystallization, Nat. Mater. 9 (2010) 1010–1014.
[31] A.F. Wallace, L.O. Hedges, A. Fernandez-Martinez, P. Raiteri, J.D. Gale, G.A. Waychunas, S. Whitelam, J.F. Banfield, J.J. De Yoreo, Microscopic Evidence for Liquid-Liquid separation in supersaturated CaCO3 solutions, Science 341 (2013) 885–889.
[32] K. Harano, T. Homma, Y. Niimi, M. Koshino, K. Suenaga, L. Leibler, E. Nakamura, Heterogeneous nucleation of organic crystals mediated by single-molecule templates, Nat. Mater. 11 (2012) 877–881.
[33] W. Pan, O. Galkin, L. Filobelo, R.L. Nagel, P.G. Vekilov, Metastable mesoscopic clusters in solutions of sickle cell hemoglobin, Biophys. J. 92 (2007) 267–277.
[34] O. Gliko, N. Neumaier, W. Pan, I. Haase, M. Fischer, A. Bacher, S. Weinkauf, P.G. Vekilov, A metastable prerequisite for the growth of lumazine synthase crystals, J. Am. Chem. Soc. 127 (2005) 3433–3438.
[35] J.R. Savage, A.D. Dinsmore, Experimental evidence for, Phys. Rev. Lett. 102 (2009) 198302.
[36] D. Maes, M.A. Vorontsova, M.A.C. Potenza, T. Sanvito, M. Sleutel, M. Giglio, P.G. Vekilov, Do protein crystals nucleate within dense liquid clusters?, Acta Crystallogr. Sect. F 71 (2015) 815–822.
[37] V. Uzunova, W. Pan, V. Lubchenko, P.G. Vekilov, Control of the nucleation of sickle cell hemoglobin polymers by free hematin, Faraday Disc. 159 (2012) 87–104.
[38] M. Sleutel, A.E. Van Driessche, Role of clusters in nonclassical nucleation and growth of protein crystals, Proc. Natl. Acad. Sci. USA 111 (2014) E546–E553.
[39] D. Kashchiev, P.G. Vekilov, A.B. Kolomeisky, Kinetics of two-step nucleation of crystals, J. Chem. Phys. 122 (2005) 244706.
[40] W. Pan, A.B. Kolomeisky, P.G. Vekilov, Nucleation of ordered solid phases of protein via a disordered high-density state: phenomenological approach, J. Chem. Phys. 122 (2005) 174905.
[41] N.E. Chayen, J.R. Helliwell, E.H. Snell, Macromolecular Crystallization and Crystal Perfection. IUCr Monographs on Crystallography, Oxford University Press, Oxford, New York, 2010, p. 24.
[42] T.H. Besseling, M. Hermes, A. Fortini, M. Dijkstra, A. Imhof, A. van Blaaderen, Oscillatory shear-induced 3D crystalline order in colloidal hard-sphere fluids, Soft Matter 8 (2012) 6931–6939.
[43] Z. Shao, J.P. Singer, Y. Liu, Z. Liu, H. Li, M. Gopinadhan, C.S. O'Hern, J. Schroers, C.O. Osuji, Shear-accelerated crystallization in a supercooled atomic liquid, Phys. Rev. E 91 (2015) 020301.
[44] B.R. Thomas, P.G. Vekilov, F. Rosenberger, Effects of microheterogeneity on hen egg white lysozyme crystallization, Acta Crystallogr. Sect. D 54 (1998) 226–236.
[45] B.R. Thomas, P.G. Vekilov, F. Rosenberger, Heterogeneity determination and purification of commercial hen egg white lysozyme, Acta Crystallogr. Sect. D 52 (1996) 776–784.
[46] M.A. Vorontsova, H.Y. Chan, V. Lubchenko, P.G. Vekilov, Lack of dependence of the sizes of the mesoscopic protein clusters on electrostatics, Biophys. J. 109 (2015) 1959–1968.
[47] Y. Li, V. Lubchenko, M.A. Vorontsova, L. Filobelo, P.G. Vekilov, Ostwald-like ripening of the anomalous mesoscopic clusters in protein solutions, J. Phys. Chem. B 116 (2012) 10657–10664.
[48] W. Pan, P.G. Vekilov, V. Lubchenko, The origin of anomalous mesoscopic phases in protein solutions, J. Phys. Chem. B 114 (2010) 7620–7630.
[49] Y. Li, V. Lubchenko, P.G. Vekilov, The use of dynamic light scattering and Brownian microscopy to characterize protein aggregation, Rev. Sci. Instrum. 82 (2011).
[50] Y. Li, V. Lubchenko, P.G. Vekilov, The use of dynamic light scattering and Brownian microscopy to characterize protein aggregation, Rev. Sci. Instr. 82 (2011) 053106.
[51] L.K. Steinrauf, Preliminary X-ray data for some new crystalline forms of -lacto-globulin and hen-egg-white lysozyme, Acta Cryst. B 12 (1959) 77–79.
[52] D.N. Petsev, X. Wu, O. Galkin, P.G. Vekilov, Thermodynamic functions of concentrated protein solutions from phase equilibria, J. Phys. Chem. B 107 (2003) 3921–3926.
[53] E. Frare, M.F. Mossuto, P.P. de Laureto, S. Tolin, L. Menzer, M. Dumoulin, C.M. Dobson, A. Fontana, Characterization of oligomeric species on the aggregation pathway of human lysozyme, J. Mol. Biol. 387 (2009) 17–27.
[54] K. Brejc, W.J. van Dijk, R.V. Klaassen, M. Schuurmans, J. van der Oost, A.B. Smit, T.K. Sixma, Crystal structure of an ACh-binding protein reveals the ligand-binding domain of nicotinic receptors, Nature 411 (2001) 269–276.
[55] R. Roxby, C. Tanford, Hydrogen ion titration curve of lysozyme in 6 M guanidine hydrochloride, Biochemistry 10 (1971) 3348–3352.
[56] Ho.Y. Chan, V. Lankevich, Peter G. Vekilov, V. Lubchenko, Anisotropy of the coulomb interaction between folded proteins: consequences for mesoscopic aggregation of lysozyme, Biophys. J. 102 (2012) 1934–1943.
[57] A. Das, C. Mukhopadhyay, Atomistic mechanism of protein denaturation by urea, J. Phys. Chem. B 112 (2008) 7903–7908.
[58] A. Caballero-Herrera, K. Nordstrand, K.D. Berndt, L. Nilsson, Effect of urea on peptide conformation in water: molecular dynamics and experimental characterization, Biophys. J. 89 (2005) 842–857.
[59] L. Hua, R. Zhou, D. Thirumalai, B.J. Berne, Urea denaturation by stronger dispersion interactions with proteins than water implies a 2-stage unfolding, Proc. Natl. Acad. Sci. USA 105 (2008) 16928–16933.
[60] M. Auton, L.M.F. Holthauzen, D.W. Bolen, Anatomy of energetic changes accompanying urea-induced protein denaturation, Proc. Natl. Acad. Sci. USA 104 (2007) 15317–15322.
[61] E.S. Courtenay, M.W. Capp, M.T. Record, Thermodynamics of interactions of urea and guanidinium salts with protein surface: relationship between solute effects on protein processes and changes in water-accessible surface area, Protein Sci. 10 (2001) 2485–2497.
[62] R.C. Diehl, E.J. Guinn, M.W. Capp, O.V. Tsodikov, M.T. Record, Quantifying additive interactions of the osmolyte proline with individual functional groups of proteins: comparisons with urea and glycine betaine, interpretation of m-values, Biochemistry 52 (2013) 5997–6010.
[63] A.S. Holehouse, K. Garai, N. Lyle, A. Vitalis, R.V. Pappu, Quantitative assessments of the distinct contributions of polypeptide backbone amides versus side chain groups to chain expansion via chemical denaturation, J. Am. Chem. Soc. 137 (2015) 2984–2995.
[64] L.B. Sagle, Y. Zhang, V.A. Litosh, X. Chen, Y. Cho, P.S. Cremer, Investigating the hydrogen-bonding model of urea denaturation, J. Am. Chem. Soc. 131 (2009) 9304–9310.
[65] S.B. Hutchens, Z.-G. Wang, Metastable cluster intermediates in the condensation of charged macromolecule solutions, J. Chem. Phys. 127 (2007) 084912.
[66] D.A. Elliott, M.T. McIntosh, H.D. Hosgood, S. Chen, G. Zhang, P. Baevova, K.A. Joiner, Four distinct pathways of hemoglobin uptake in the malaria parasite Plasmodium falciparum, Proc. Natl. Acad. Sci. USA 105 (2008) 2463–2468.
[67] P.G. Vekilov, M.A. Vorontsova, Nucleation precursors in protein crystallization, Acta Crystallogr. F. Struct. Biol. Cryst. Commun. 70 (2014) 271–282.
[68] J.F. Lutsko, G. Nicolis, Mechanism for the stabilization of protein clusters above the solubility curve, Soft Matter 12 (2015) 93–98.
[69] J. Wang, M. Dauter, R. Alkire, A. Joachimiak, Z. Dauter, Triclinic lysozyme at 0.65 A resolution, Acta Crystallogr. Sect. D 63 (2007) 1254–1268.
[70] J.A. McCammon, B.R. Gelin, M. Karplus, P.G. Wolynes, The hinge-bending mode of lysozyme, Nature 262 (1976) 325–326.
[71] H.R. Ibrahim, T. Matsuzaki, T. Aoki, Genetic evidence that antibacterial activity of lysozyme is independent of its catalytic function, FEBS Lett. 506 (2001) 27–32.
[72] O.K. Gasymov, B.J. Glasgow, ANS fluorescence: potential to Augment the Identification of the external binding sites ofProteins, Biochim. Et. Biophys. Acta 1774 (2007) 403–411.
[73] A. Hawe, M. Sutter, W. Jiskoot, Extrinsic fluorescent dyes as tools for protein characterization, Pharm. Res. 25 (2008) 1487–1499.
[74] M. Biancalana, S. Koide, Molecular mechanism of Thioflavin-T binding to Amyloid fibrils, Biochim. Et. Biophys. Acta 1804 (2010) 1405–1412.